

NOTES AND CORRESPONDENCE

Application of a Subfilter-Scale Flux Model over the Ocean Using OHATS Field Data

MARK KELLY*

Department of Meteorology, The Pennsylvania State University, University Park, Pennsylvania

JOHN C. WYNGAARD

Department of Meteorology, and Department of Mechanical Engineering, The Pennsylvania State University, University Park, Pennsylvania

PETER P. SULLIVAN

Mesoscale and Microscale Meteorology Group, National Center for Atmospheric Research, Boulder, Colorado

(Manuscript received 28 July 2008, in final form 9 March 2009)

ABSTRACT

Simple rate equation models for subfilter-scale scalar and momentum fluxes have previously been developed for application in the so-called “terra incognita” of atmospheric simulations, where the model resolution is comparable to the scale of turbulence. The models performed well over land, but only the scalar flux model appeared to perform adequately over the ocean. Analysis of data from the Ocean Horizontal Array Turbulence Study (OHATS) reveals a need to account for the moving ocean–air interface in the subfilter stress model. The authors develop simple parameterizations for the effect of surface-induced pressure fluctuations on the subfilter stress, leading to good predictions of subfilter momentum flux both over land and in OHATS.

1. Introduction

Modeling of the turbulent atmospheric boundary layer (ABL) has improved continuously in the four decades since the first computer simulations of atmospheric flows, with enormous increases in computing power along the way. But computational limitations still require that atmospheric simulations use filtered equations, retaining scales larger than the filter scale Δ_f . So-called subfilter-scale (SFS) or “unresolvable” quantities, which involve scales smaller than Δ_f , often carry significant fluxes of momentum, heat, kinetic energy, and scalar constituents (such as water vapor), particularly near surfaces and interfaces; such fluxes must be mod-

eled (e.g., Bryan et al. 2003; Sullivan et al. 2003). Subfilter models use resolvable fields to parameterize the relevant dynamics and processes occurring at unresolved scales and thus have an implicit—and often unacknowledged—dependence upon the filter scale (Wyngaard 2004). Both mesoscale simulation, which calculates fields at scales much larger than the energy-containing turbulence scale ℓ , and large-eddy simulation (LES), which resolves scales on the order of ℓ and smaller, have become common tools in the study of the atmosphere, evolving to the point that each has its own set of commonly used SFS models. Mesoscale and large-eddy simulations of the atmosphere each employ SFS models of physics at scales smaller than the filter scale Δ_f , but in general SFS models used for mesoscale simulations are not appropriate for use in LES, and vice versa. The established SFS models employed in the mesoscale regime ($\ell \ll \Delta_f$) and LES regime ($\ell \gg \Delta_f$) are mostly inappropriate for the intermediate regime in which ℓ and Δ_f have the same order of magnitude, as discussed by Wyngaard (2004). In this “terra incognita,” where large-domain LES and fine-resolution mesoscale

* Current affiliation: Wind Energy Division, Risø National Lab/Danish Technical University, Roskilde, Denmark.

Corresponding author address: Mark Kelly, Wind Energy Division, Risø National Lab/Danish Technical University, Roskilde 4000, Denmark.
E-mail: mark.c.kelly@risoe.dk

simulations begin to overlap, he suggested that SFS stress and flux rate equation models be used.

Hatlee and Wyngaard (2007) demonstrated that the rate equation model of Wyngaard (2004) predicted the subfilter heat fluxes measured over land during the Horizontal Array Turbulence Study (HATS; Sullivan et al. 2003). They also developed an improved model for SFS stresses. We find that data from the Ocean Horizontal Array Turbulence Study (OHATS) indicate that the effects of pressure fluctuations induced by the moving surface waves must be included in the modeled SFS stress budget; this is consistent with the measurements of Sjöblom and Smedman (2003) and the simulations of Sullivan and McWilliams (2002), with the latter indicating that wave-induced pressures can exceed turbulent pressure fluctuations ($\sim \rho u_*^2$) by an order of magnitude during typical conditions over the ocean. We develop simple parameterizations for such effects, working toward a generalization of the Hatlee and Wyngaard (2007) model.

2. Subfilter flux measurements and model

Using the data from both HATS and OHATS, we first examine the performance of the Hatlee and Wyngaard (2007) subfilter flux model over land and sea. Comparison of results in these two regimes leads us to extend the model for use over the ocean.

a. Over-sea measurements from OHATS

The Ocean Horizontal Array Turbulence Study employed two parallel horizontal rows of nine sonic anemometers mounted on the Air–Sea Interaction Tower of the Martha’s Vineyard Coastal Observatory (Sullivan et al. 2006), that is, essentially the HATS setup over the ocean. As in HATS (Sullivan et al. 2003) the arrays are separated in the vertical and situated roughly perpendicular to the prevailing wind, permitting filtering in both horizontal directions (Tong et al. 1998)¹ and differentiation of filtered quantities in three dimensions; this facilitates the measurement of resolved fields used by atmospheric simulations and of subfilter fluxes, which must be parameterized in such simulations. The OHATS arrays were located 5 and 5.58 m from the mean ocean surface level, with both arrays having uniform lateral spacing with $\Delta_y = 0.58$ m and a filter scale $\Delta_f = 4\Delta_y$ (this Δ_f corresponds to the use of five contiguous anemometers for lateral filtering and allows double-filtering over an array). In OHATS the time-varying wave height was also measured by three downward-facing laser altimeters

¹ Tong et al. (1998, 1999) showed that filtering in the two horizontal directions is an acceptable approximation for three-dimensional filtering in the lower atmospheric boundary layer.

situated above a mean ocean depth of 15.6 m (for details, see Sullivan et al. 2006; Edson et al. 2007). The sonic anemometers measure the three velocity components u_i and provide the potential temperature θ ;² however, the anemometers’ high-humidity correction algorithms degraded the measurements of mean temperature, so the mean temperatures for each 30-min data period were corrected.³

b. Wave-correlated fields

To examine the influence of surface waves, we use the Hristov et al. (1998) algorithm with recorded time series of wave heights to calculate the wave-correlated components (u_i^w, θ^w) of the measured fields (u_i, θ). This method permits isolation of a finite-bandwidth “wavy” component from a time series given an arbitrary wave signal, such that the wavy and turbulent components are completely uncorrelated (e.g., $u_i = u_i^w + u_i^t$ where u_i^t is the turbulent part).

In OHATS, the wave-correlated components of the horizontal velocity and temperature fields (u_1^w, u_2^w, θ^w) are much smaller than the total fluctuations of these fields. However, the influence of waves is evident in the vertical velocity field u_3 , as seen in the spectra of wavy and full u_3 presented in Fig. 1; we found rms amplitudes⁴ of wave-correlated vertical velocities as large as one third of the corresponding turbulent amplitudes. But the wave-correlated vertical velocities are not large enough to significantly affect the measurable second-order quantities ($u_i u_j, u_i \theta$) that comprise the SFS fluxes, and the measured *subfilter fluxes* themselves contain only small wave-correlated fluctuations (in fact, the results presented here were not greatly affected by removal of the wave-correlated portion of u_i and θ). Such a situation is understandable given that much of the OHATS data is dominated by swell conditions, with spectral content below 0.2 Hz, as shown in Fig. 1c. Rieder and Smith (1998) pointed out that stress in the ~ 0.06 – 0.16 -Hz band is controlled by swell, which for the observed wave spectra peaks f_{peak} in this band and wave (phase) speeds of $c_p \sim 4$ – 12 m s⁻¹ corresponds roughly to scales

² The sonic anemometers measure temperature via the temperature dependence of the speed of sound, yielding a “sonic temperature” $T_c \simeq T(1 + 0.51q_v)$ that depends on specific humidity q_v , similar to virtual temperature.

³ For each 10-min measurement period, $\overline{d\theta/dz}$ was recalculated via the measured heat and moment flux at each height, using the Dyer and Hicks (1970) empirical similarity expression for dimensionless temperature gradient.

⁴ Root-mean-square and other ensemble mean quantities are approximated by time averages for each 30-min data period, unless otherwise noted.

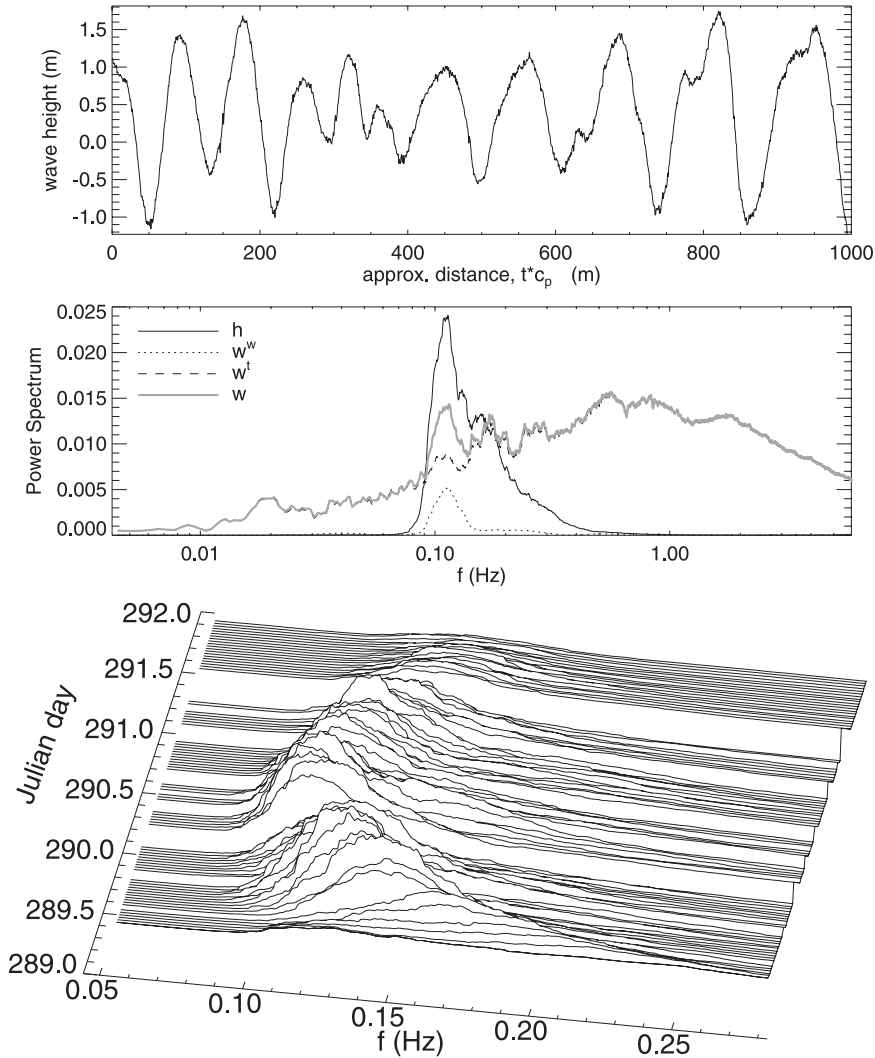


FIG. 1. (top) Sample 60-s record of surface wave height; horizontal extent of waves approximated as the product of time t and wave speed c_p (calculated from peak frequency of wave spectrum). (middle) The corresponding one-dimensional power spectra of surface height h (dark solid), vertical velocity w (light thick), turbulent part w' (dashed), and wave-correlated part w^w (dot-dashed) from OHATS, 8:30–9:00 a.m. 17 Oct 2004. (bottom) One-dimensional wave spectra for the last 60 h (16–18 October) of OHATS.

of $\sim c_p/f_{\text{peak}}$ ($\sim 25\text{--}150$ m)—much larger than the filter scale of $\Delta_f \sim 2.3$ m. Consequently, we postulate that the ocean affects the measured SFS fluxes predominantly through wave-induced pressure and perhaps its aggregate effect on mean gradients, but because the OHATS data do not include measurements of fluctuating pressure we must infer the extent of its influence.

1) SUBFILTER TEMPERATURE FLUX

The subfilter flux f_i of a conserved scalar such as potential temperature θ is defined by

$$f_i = \overline{u_i \theta} - \overline{u_i} \overline{\theta}, \tag{1}$$

with overbars denoting spatial averages over extent Δ_f . The conservation equation for f_i is (Wyngaard 2004)

$$\begin{aligned} \frac{\partial f_i}{\partial t} + \overline{u_j} \frac{\partial f_i}{\partial x_j} = & -\frac{\partial}{\partial x_j} (\overline{\theta u_i u_j} - \overline{\theta u_i} \overline{u_j} - \overline{\theta u_i u_j} - \overline{u_i \theta u_j} + 2\overline{\theta u_i} \overline{u_j}) - \frac{1}{\rho} \frac{\partial}{\partial x_i} (\overline{p \theta} - \overline{p} \overline{\theta}) - f_j \frac{\partial \overline{u_i}}{\partial x_j} \\ & - R_{ij} \frac{\partial \overline{\theta}}{\partial x_j} + \frac{1}{\rho} \left(\overline{p} \frac{\partial \overline{\theta}}{\partial x_i} - \overline{p} \frac{\partial \overline{\theta}}{\partial x_i} \right) + \delta_{i3} \frac{g}{\theta_0} (\overline{\theta \theta} - \overline{\theta} \overline{\theta}). \end{aligned} \tag{2}$$

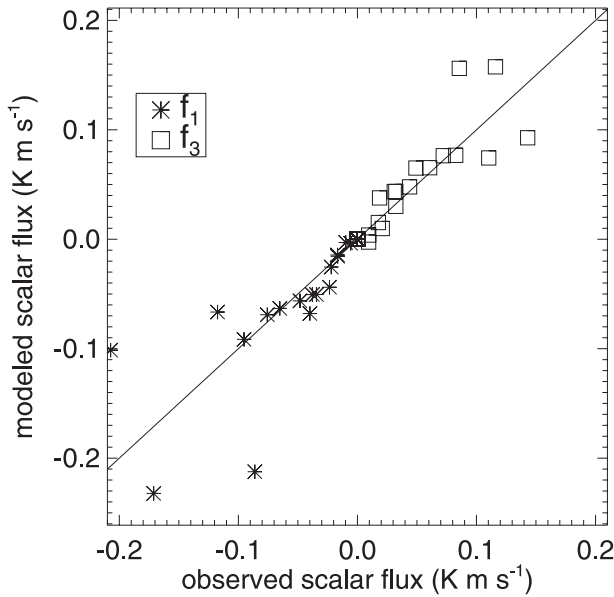


FIG. 2. Wyngaard (2004) model (3) vs observations of subfilter heat flux f_i for HATS.

The terms on the left are local time change and advection by the resolved field; those on the right are turbulent transport, pressure transport, tilting production, gradient production, pressure destruction, and buoyant production; $R_{ij} \equiv \overline{u_i u_j} - \overline{u_i} \overline{u_j}$ is the kinematic Reynolds stress.

Wyngaard (2004) retained the tilting production, gradient production, and pressure-destruction terms in Eq. (2) to produce the rate equation model

$$\frac{\partial f_i}{\partial t} = -f_j \frac{\partial \overline{u_i}}{\partial x_j} - R_{ij} \frac{\partial \overline{\theta}}{\partial x_j} - \frac{f_i}{T}. \quad (3)$$

The last term ($-f_i/T$) is a parameterization of the pressure-destruction term, and is an adaptation of the Rotta (1951) model used in second-order closure. We take the time scale T as $T \equiv C_\theta \Delta_f / e^{1/2}$, where $e \equiv \frac{1}{2}(\overline{u_k u_k} - \overline{u_k} \overline{u_k})$ is the SFS turbulent kinetic energy and C_θ is a constant equal to 0.30 (Hatlee and Wyngaard 2007).

The quasi-steady model implied by Eq. (3) is

$$f_i = -T f_j \frac{\partial \overline{u_i}}{\partial x_j} - T R_{ij} \frac{\partial \overline{\theta}}{\partial x_j}, \quad (4)$$

while the “standard” model used frequently in meso-scale and large-eddy simulations is

$$f_i = -K \frac{\partial \overline{\theta}}{\partial x_i}, \quad (5)$$

with $K \simeq e^{1/2} \Delta_f$ being a subgrid eddy diffusivity. The model (4) differs from (5) in two important ways: Eq. (4) in effect relates f_i to $\partial \overline{\theta} / \partial x_j$ with a tensor eddy diffusivity ($\sim T R_{0j} + \dots$) whereas the standard model (5) has a scalar diffusivity K ; also, the model (4) has an addi-

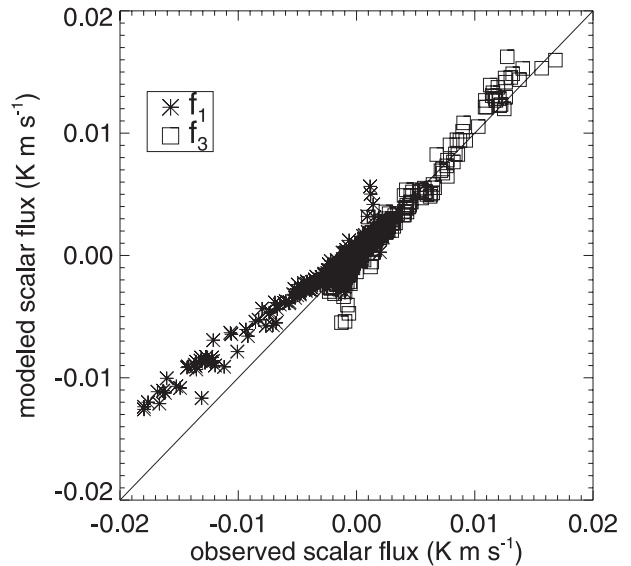


FIG. 3. Wyngaard (2004) model (3) vs observations of subfilter heat flux f_i from OHATS.

tional term representing the effects of tilting production. Wyngaard (2004) found, and Hatlee and Wyngaard (2007) confirmed, that this additional term is important for representing the horizontal flux, which is produced by tilting and by the tensor diffusivity.

The predictions of the model (3) generally match the HATS overland observations in unstable conditions (Hatlee and Wyngaard 2007), as shown in Fig. 2. They found that adding stochastic advection to (3) increased SFS flux fluctuations and that inclusion of turbulent transport and buoyancy terms did not appreciably affect (3).

For OHATS the model (3) gives less scatter than over land, but with some systematic bias in predictions; this is shown in Fig. 3. The slight underprediction of horizontal flux magnitude could be due in part to the reduced mean shear caused by the influence of ocean waves (Smedman et al. 1999; Sullivan et al. 2008)—particularly during swell-dominated conditions (Sjöblom and Smedman 2003), which were common during OHATS. This would act to decrease the “tilting” term ($-f_3 \partial \overline{u_1} / \partial z$). The slight overprediction of f_3 could be related to the correction to $\langle \theta \rangle$ or the moving surface; in light of this correction, the surface’s unmodeled impact on f_i is small enough that we do not attempt to parameterize surface-induced pressure effects in (3).

The higher mean wind speeds U in OHATS relative to HATS caused larger effective streamwise differencing intervals $\Delta x \simeq U \Delta t$ and, hence, reduced the accuracy of x derivatives calculated by finite-differencing. For the anemometer sampling interval $\Delta t = 0.05$ s and filter width Δ_f in OHATS, when $U \gtrsim 10$ m s $^{-1}$ the number of streamwise filter points is limited to $n_x = \Delta_f / (U \Delta t) \leq 5$;

this minor effect was reduced with modestly axisymmetric filtering⁵ for the data in Fig. 3.

2) SUBFILTER MOMENTUM FLUX: DEVIATORIC STRESS

The deviatoric subfilter kinematic stress is the zero-trace ($\tau_{ii} = 0$) tensor

$$\begin{aligned} \frac{\partial \tau_{ij}}{\partial t} + \bar{u}_k \frac{\partial \tau_{ij}}{\partial x_k} &= \frac{\partial}{\partial x_k} \left[\overline{u_i u_j u_k} - \bar{u}_i \bar{u}_j \bar{u}_k - \bar{u}_j \bar{u}_i \bar{u}_k - \bar{u}_k \bar{u}_i \bar{u}_j + 2\bar{u}_i \bar{u}_j \bar{u}_k - \frac{1}{3} \delta_{ij} (\overline{u_l^2 u_k} - 2\bar{u}_l \bar{u}_l \bar{u}_k - \bar{u}_k \bar{u}_l^2 + 2\bar{u}_l^2 \bar{u}_k) \right] \\ &+ \frac{4}{3} e \bar{S}_{ij} - \left(\tau_{jk} \frac{\partial \bar{u}_i}{\partial x_k} + \tau_{ik} \frac{\partial \bar{u}_j}{\partial x_k} - \frac{2}{3} \delta_{ij} \tau_{kl} \bar{S}_{kl} \right) - \frac{2}{\rho} (\bar{p} \bar{S}_{ij} - \bar{p} \bar{S}_{ij}) \\ &+ \frac{1}{\rho} \frac{\partial}{\partial x_k} \left[\delta_{ik} (\bar{u}_j \bar{p} - \bar{u}_j \bar{p}) + \delta_{jk} (\bar{u}_i \bar{p} - \bar{u}_i \bar{p}) - \frac{2}{3} \delta_{ij} (\bar{u}_k \bar{p} - \bar{u}_k \bar{p}) \right], \end{aligned} \quad (6)$$

where the resolved strain rate is $\bar{S}_{ij} \equiv 1/2(\partial \bar{u}_i / \partial x_j + \partial \bar{u}_j / \partial x_i)$. The terms on the left are local time change and advection by the resolved field; on the right are turbulent transport, isotropic production, deviatoric production, pressure destruction, and pressure transport. The Hatlee and Wyngaard (2007) “simple” model for τ_{ij} is

$$\frac{\partial \tau_{ij}}{\partial t} = \frac{4}{3} e \bar{S}_{ij} - \left(\tau_{jk} \frac{\partial \bar{u}_i}{\partial x_k} + \tau_{ik} \frac{\partial \bar{u}_j}{\partial x_k} - \frac{2}{3} \delta_{ij} \tau_{kl} \bar{S}_{kl} \right) - \frac{\tau_{ij}}{T_\tau}. \quad (7)$$

This model is analogous to the model (3) for SFS scalar flux in retaining only the key terms in the conservation equation. Here these are isotropic production and deviatoric production, which are represented explicitly, and pressure destruction, which is modeled with the Rotta-type term $-\tau_{ij}/T_\tau$. The time scale T_τ is again of the form $C_\tau \Delta_f e^{-1/2}$.

The Lilly (1967) “first-order theory” for τ_{ij} is

$$\tau_{ij} = K \bar{S}_{ij}, \quad (8)$$

which today is generally called the Smagorinsky model; it ignores the deviatoric production terms in the τ_{ij} conservation equation.

Hatlee and Wyngaard (2007) showed with the HATS data that the model (7) is a vast improvement over the Smagorinsky model (8), most closely matching the observations when the constant C_τ is chosen to be 0.18; however, for this value of C_τ the model (7) overpredicts the rate of energy transfer from resolved to subfilter scales. To remedy this, Hatlee and Wyngaard (2007)

$$\begin{aligned} \tau_{ij} &\equiv - \left[\overline{u_i u_j} - \bar{u}_i \bar{u}_j - \frac{1}{3} \delta_{ij} (\overline{u_k u_k} - \bar{u}_k \bar{u}_k) \right] \\ &= - (R_{ij} - \frac{2}{3} \delta_{ij} e). \end{aligned}$$

Its conservation equation is (Lilly 1967; Hatlee and Wyngaard 2007)

extended the model (7) to include a parameterization for the mean-shear contribution Π_{ij}^S to the SFS pressure-strain tensor $\Pi_{ij} \equiv -2\rho^{-1}(\bar{p} \bar{S}_{ij} - \bar{p} \bar{S}_{ij})$:

$$\begin{aligned} \Pi_{11}^S &= -\Pi_{33}^S = C_{11} e^{1/2} \Delta_f \left(\frac{\partial U}{\partial z} \right)^2, \\ \Pi_{13}^S &= C_{13} e \frac{\partial U}{\partial z}, \quad \Pi_{22}^S = 0, \end{aligned} \quad (9)$$

which when added to the simple model (7) gives their “full” model,

$$\begin{aligned} \frac{\partial \tau_{ij}}{\partial t} &= \frac{4}{3} e \bar{S}_{ij} - \left(\tau_{jk} \frac{\partial \bar{u}_i}{\partial x_k} + \tau_{ik} \frac{\partial \bar{u}_j}{\partial x_k} - \frac{2}{3} \delta_{ij} \tau_{kl} \bar{S}_{kl} \right) \\ &- \frac{\tau_{ij}}{T_\tau} + \Pi_{ij}^S. \end{aligned} \quad (10)$$

They found that (10) gives good predictions of both τ_{ij} and downscale TKE transfer in HATS, using the constants $C_{13} = C_{11} = 0.4$ and $C_\tau = 0.08$.

For OHATS, however, the Hatlee and Wyngaard (2007) model (10) performed poorly, as indicated by Fig. 4. The figure shows systematic underprediction of the magnitudes of the deviatoric normal stresses $\tau_{\alpha\alpha}$ by a factor of 3 and overprediction of the shear stress τ_{13} by 10%–50%.⁶ Physically, the latter effect is due to the wind “following” the waves: in OHATS the waves on average are moving faster than the air above, inducing pressure fluctuations that help drive the wind. This in effect transfers momentum from sea to air—opposing the

⁵ This can be alleviated through axisymmetric filtering, where the streamwise filter width Δ_x is larger than the lateral width Δ_y , and the effective filter width Δ_f is taken to be $(\Delta_x \Delta_y)^{1/2}$. For Fig. 3 we used $\Delta_x = 2\Delta_y$.

⁶ The streamwise resolution limitation caused by large wind speeds was mitigated through axisymmetric filtering; due to the extra streamwise derivative in Π_{11}^S relative to the other Π_{ij}^S , modeled Π_{11}^S was divided by the factor Δ_x/Δ_y , giving consistent results over varying filter aspect ratios Δ_x/Δ_y . For stress we show results calculated with a symmetric filter, $\Delta_x = \Delta_y = \Delta_f$.

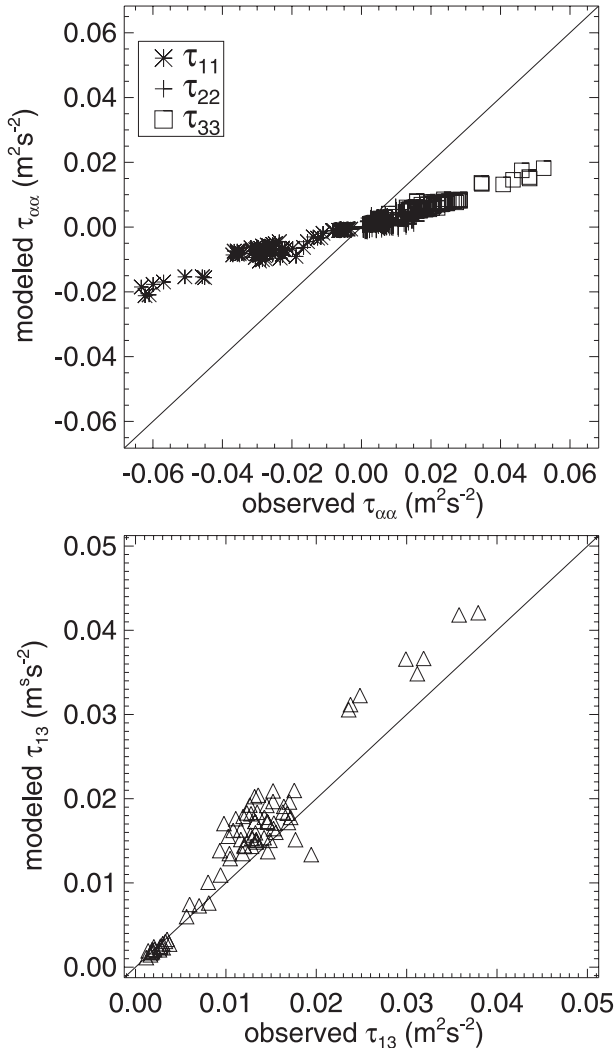


FIG. 4. Subfilter deviatoric stress model (10) including rapid pressure model (14) vs observed τ_{ij} for OHATS: (top) Normal stresses, $\tau_{\alpha\alpha}$; (bottom) shear stress τ_{13} .

usual turbulent momentum flux associated with the surface—and reduces the mean shear $\partial U/\partial z$ (Sullivan et al. 2008); such a phenomenon has been found both in simulations (Sullivan and McWilliams 2002) and observations (e.g., Grachev and Fairall 2001). The underpredictions of $\tau_{\alpha\alpha}$ —i.e., of the deviations of the normal SFS stresses from isotropy—are presumably due to redistribution of SFS energy by surface-induced pressure fluctuations. The failure of (10) in OHATS suggests a need to account for the moving wavy surface, particularly over swell-dominated seas.

c. Modeling of surface-induced pressure contribution to τ_{ij}

The previous section included a parameterization (9) for the subfilter covariance of strain rate S_{ij} and mean-

shear component of pressure p_s , following from solution of the mean-shear component of the Poisson equation. But solution of the Poisson equation in a half-space also includes a surface integral

$$p_{\text{bnd}}(\mathbf{x}) = \iint_{S'} \frac{\partial}{\partial n} [p(\mathbf{x}, \mathbf{x}') G(\mathbf{x}, \mathbf{x}')] dS', \quad (11)$$

with n normal to the surface. For filter scales in the terra incognita of atmospheric simulations ($\Delta_f \sim 50\text{--}500$ m), p_{bnd} is negligible over land but must be modeled over the ocean. A relatively simple parameterization for the ocean-induced contribution to Π_{ij} follows from an estimate for the pressure induced by the moving air–sea interface. Theoretically, a Green’s function $G(\mathbf{x}, \mathbf{x}')$ could be chosen such that the integrand of (11) reduces to $G(\mathbf{x}, \mathbf{x}') \partial p(\mathbf{x}, \mathbf{x}')/\partial n$, requiring the specification of an (average) effective kinematic force $\partial p/\partial n$ with which the waves “push” the air; but this is difficult in practice—particularly over a time-varying wave field with significant spectral width—so we resort to a crude energy argument to estimate p_{bnd} . Assuming that the rate of work done by the ocean is on average proportional to $p_{\text{bnd}}(z)$, and that this power input is some fraction of the dissipation rate ε , we take $p_{\text{bnd}} \propto \varepsilon \propto e^{3/2}$. Then following the Plant (1982) and Smith et al. (1992) findings that overseas drag coefficients or ocean-induced pressure drag (“form drag”) are proportional to the wave age c_p/U , we propose the form⁷

$$\Pi_{ij}^{\text{sfc}} = C_{ij}^{\text{sfc}} \left(\frac{e}{g\lambda}\right)^{1/2} \left(\frac{c_p}{U}\right) e \bar{S}_{ij} \quad (12)$$

for the surface-induced SFS pressure strain, where we use $\Pi_{22}^{\text{sfc}} = -\Pi_{11}^{\text{sfc}} - \Pi_{33}^{\text{sfc}}$ and set $C_{12}^{\text{sfc}} = C_{23}^{\text{sfc}} = 0$, with λ being the dominant (peak) wavelength.

Although Janssen (1999) found the covariance of pressure and vertical velocity to be significantly influenced by the wind-wave angle, and Vickers and Mahrt (1997) suggested that wave spectral *width* dominates the drag coefficient rather than the wave age (spectral peak), the parameterization (12) is consistent with the normal deviatoric stresses observed during OHATS. For example, Fig. 5 shows τ_{11} to be linearly dependent on wave age c_p/U for $c_p/U \gtrsim 1.5$, presumably swell-dominated conditions. For smaller wave ages⁸ and waves

⁷ The wave age is typically defined using U_{10} (the mean wind 10 m above the water), often incorporating the wind-wave angle α by using $U_{10} \cos \alpha$. But OHATS gave U at only 5–5.6 m, and for generality, we use U here.

⁸ The cluster of points in the left corner of Fig. 5 is likely due to the minority of conditions with an appreciable wind-wave angle, where c_p/U tended to be small.

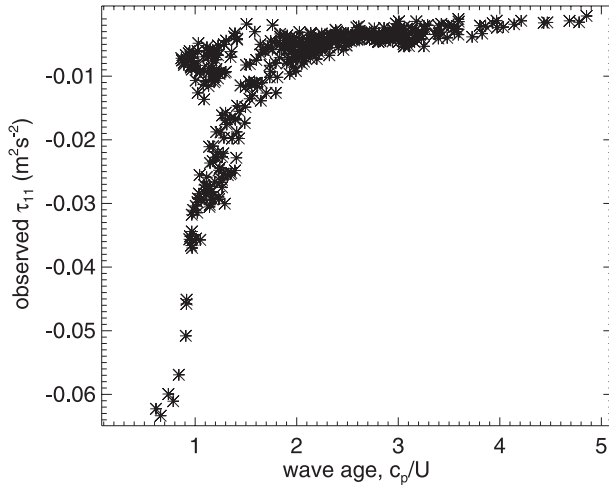


FIG. 5. Normal subfilter deviatoric stress $\tau_{11} \equiv -[R_{11} - (2/3)e]$ vs wave age observed during OHATS; U taken at $z = 5$ m.

following the wind ($c_p < U$), the parameterization (12) has diminishing impact on modeled τ_{ij} ; the surface-induced pressure will have a smaller effect on the stress, and the model (10) should perform well even without Π_{11}^{sfc} .

For each 30-min OHATS data segment we calculate the mean wave speed c_p from the peak frequency wave-height spectrum by applying Newton–Raphson iteration to the dispersion relation $c_p = (g/\omega_{\text{peak}}) \tanh(\omega_{\text{peak}}d/c_p)$, with water depth $d = 15.6$ m and $\omega_{\text{peak}} = 2\pi f_{\text{peak}}$; again, the subfilter energy e is diagnosed from measurements as in Hatlee and Wyngaard (2007). For OHATS a relatively wide range of coefficients C_{ij}^{sfc} give marked improvement over the land-based model (10); the data suggest⁹ $\{C_{11}^{\text{sfc}}, C_{13}^{\text{sfc}}, C_{33}^{\text{sfc}}\} \approx \{-30, -5, 10\} \pm 25\%$. Figure 6 displays the results of adding the surface pressure parameterization (12) to the rate equation model (10), showing a dramatic improvement over this land-based model (Fig. 4).¹⁰ Figure 6 also shows that (12) leads to more precise predictions than over flat land in HATS; this is likely due to the relatively large influence of the waves, and the ranges of ℓ/Δ_f and atmospheric stability z/L_{MO} (where L_{MO} is the Monin–Obukhov length) being significantly narrower in OHATS than in HATS.

⁹ Echoing the height dependence of pressure, a factor like $\exp(-az/\lambda)$ (Hasselmann and Bösenberg 1991) could be included in C_{ij}^{sfc} . For simplicity we refrain from doing so, both because e decreases (implicitly) with z and because data were taken at only two heights.

¹⁰ For the figure we use our modified form of the mean-shear contribution Π_{ij}^{sfc} , Eq. (14), with $C_\tau = 0.10$ and $C_{13} = 0.5$ (see next section).

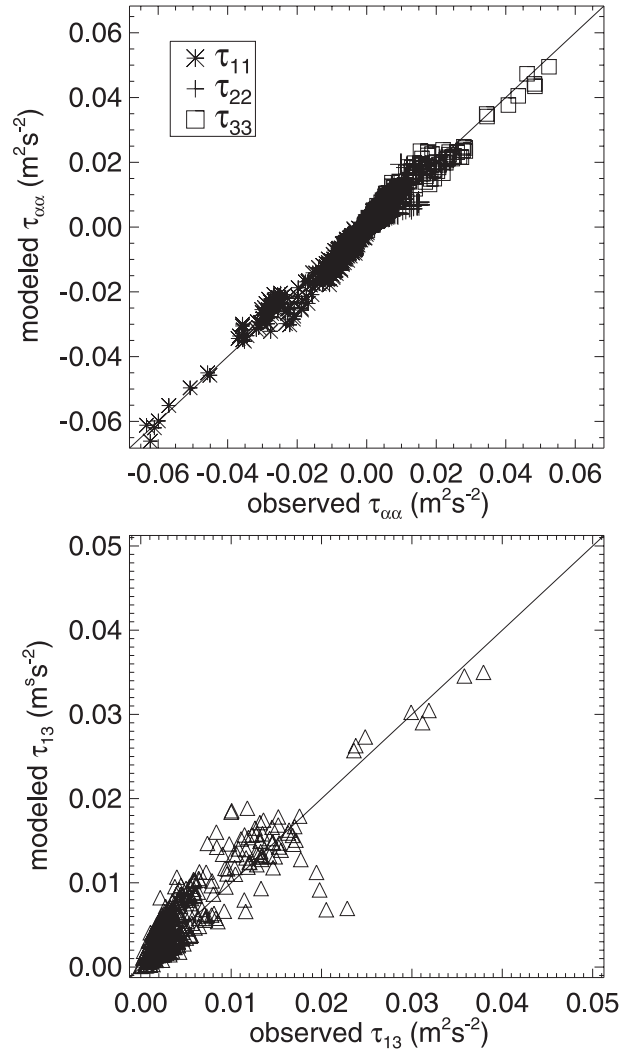


FIG. 6. Predictions of model [(10) and (14)] plus surface-induced pressure-strain parameterization (12) for subfilter stress τ_{ij} vs observations in OHATS: (top) Normal stresses, $\tau_{\alpha\alpha}$; (bottom) shear stress τ_{13} . Here $C_{11}^w = -28$, $C_{13}^w = 5$, $C_{33}^w = 10$.

An alternative model for Π_{ij}^{sfc} is also derived by adapting the empirically determined drag coefficient relation $C_D(u_*/g, \omega_{\text{peak}})$ of Hwang (2004) to parameterize the contribution of ocean-induced pressure to τ_{ij} . Using data from a number of different measurement campaigns, Hwang (2004) found the drag coefficient C_D at height $z = \lambda/2$ (half the representative wavelength) to behave as $C_{\lambda/2} \propto (\omega_{\text{peak}}u_*/g)^{0.7}$, where $u_* \equiv \langle -uw \rangle^{1/2}$ is the friction velocity. Now replacing u_* with $e^{1/2}$ and estimating the subfilter part of $p_{\text{bnd}}S_{ij}$ to behave as $C_D e \bar{S}_{ij}$, considering the general form of Π_{ij} we arrive at the relation

$$\Pi_{ij}^{\text{sfc}} = C_{ij}^{\text{sfc}} \left(\frac{\omega_{\text{peak}} e^{1/2}}{g} \right)^{0.7} e \bar{S}_{ij}. \quad (13)$$

Using $C_{ij}^{sfc'} = 0.2C_{ij}^{sfc}$, the parameterization (13) added to the rate equation model (10) gives τ_{ij} very similar to the values predicted using (12), so that the results appear identical to Fig. 6. Such results are understandable given that (13) has a dependence $\Pi_{ij}^{sfc} \propto e^{1.35}$ similar to the $e^{1.5}$ dependence of (12).¹¹ The form (12) is essentially a low-order approximation for wave effects that are likely characterized by more parameters than just wave age; more accurate or higher-order parameterizations could contain a dependence on wind-wave angle and stability, but that is beyond the scope of this note.

We also found that increasing the constant C_τ to 0.10 improved predictions of τ_{ij} in HATS, along with increasing C_{13} to 0.5. The rapid-shear model was further improved by using the arguments of Hatlee and Wyngaard (2007, their appendix A) to set

$$\begin{aligned} \Pi_{33}^S &= 0.8e \frac{\partial U}{\partial z}, & \Pi_{22}^S &= -\Pi_{11}^S - \Pi_{33}^S, \\ \Pi_{11}^S &= C_{11} e^{1/2} \Delta_f \left(\frac{\partial U}{\partial z} \right)^2, & \Pi_{13}^S &= C_{13} e \frac{\partial U}{\partial z}, & \text{and} \\ \Pi_{12}^S &= 0, \end{aligned} \tag{14}$$

where the second line of (14) is the same as for (9). This choice for Π_{33}^S permits nonzero Π_{22}^S and allows for the possibility that the behaviors of Π_{11}^S and Π_{33}^S differ more over waves than over land. Indeed, we find that it reduces the scatter in OHATS predictions, and it was used in the model for the data shown in Fig. 6. Predictions using our modified mean-shear parameterization (14) are compared to HATS observations in Fig. 7 (bottom), which shows some improvement over the Hatlee and Wyngaard (2007) mean-shear form (9).

3. Summary

Here we have developed simple parameterizations for the effect of ocean-induced pressure on subfilter stress and refined the Hatlee and Wyngaard (2007) form for pressure strain in order to generalize the Hatlee and Wyngaard (2007) SFS flux model for use over sea and land. The new parameterizations greatly improve predictions of stress for data from the Ocean Horizontal Array Turbulence Study (OHATS).

The characterization and testing of the parameterizations for the pressure effects of the moving ocean-

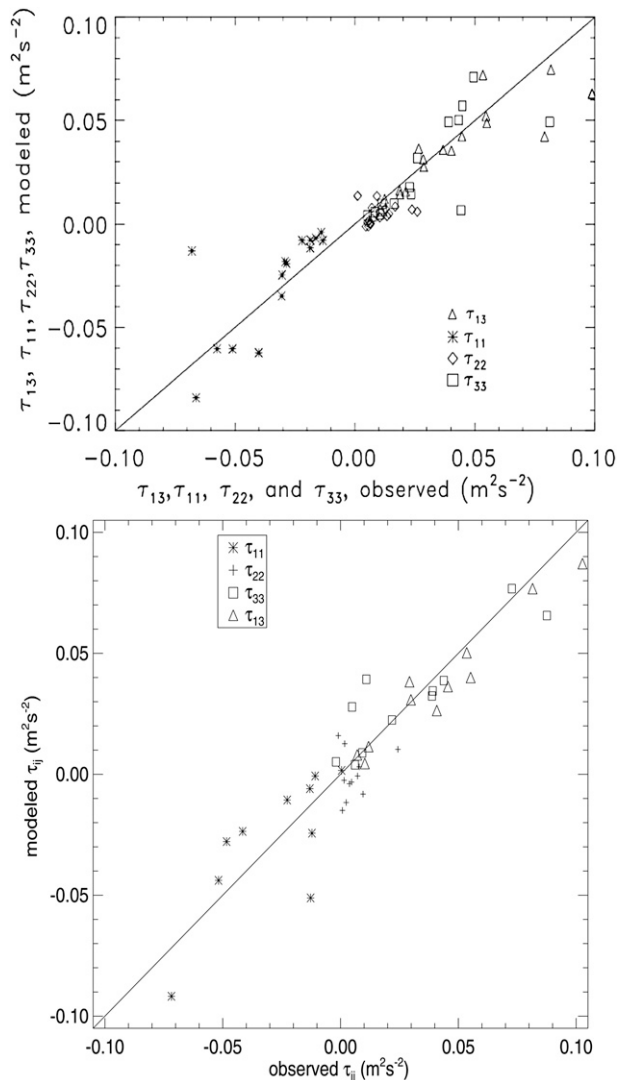


FIG. 7. Modeled vs observed τ_{ij} from HATS. (top) Hatlee and Wyngaard (2007) model (9) results (their Fig. 11); (bottom) new model (14).

air interface were limited by a number of factors. The OHATS data were taken over a relatively narrow range of l/Δ_f and stabilities z/L_{MO} compared to HATS, with streamwise filtering issues incurred by wind speeds greater than 10% of the product of filter width Δ_f and anemometer sample rate. The corrections made to $\langle \theta \rangle$ also limit the analysis of subfilter potential temperature flux. The models (12) and (13) for ocean-induced subfilter pressure strain are compatible and perform rather well for OHATS, but more marine boundary layer data—including pressure measurements—are needed to investigate the dependence of ocean-induced pressure strain on altitude, wave slope, stability, or other parameters.

¹¹ A factor λ/z may also be appropriate in (13), and we found that including it (with the adjustment $C_{ij}^{sfc'} \approx C_{ij}^{sfc}/75$) produces effectively identical results; however, because OHATS has measurements taken at essentially one height ($\pm \sim 10\%$) we omit such a dependence.

Acknowledgments. This work was supported in part by NSF Award Number 0349410.

REFERENCES

- Bryan, G. H., J. C. Wyngaard, and J. M. Fritsch, 2003: Resolution requirements for the simulation of deep moist convection. *Mon. Wea. Rev.*, **131**, 2394–2416.
- Dyer, A., and B. Hicks, 1970: Flux-gradient relationships in the constant flux layer. *Quart. J. Roy. Meteor. Soc.*, **96**, 715–721.
- Edson, J. B., and Coauthors, 2007: The coupled boundary layers and air–sea transfer experiment in low winds. *Bull. Amer. Meteor. Soc.*, **88**, 341–356.
- Grachev, A. A., and C. W. Fairall, 2001: Upward momentum transfer in the marine boundary layer. *J. Phys. Oceanogr.*, **31**, 1698–1711.
- Hasselmann, D., and J. Bösenberg, 1991: Field measurements of wave-induced pressure over wind-sea and swell. *J. Fluid Mech.*, **230**, 391–428.
- Hatlee, S. C., and J. C. Wyngaard, 2007: Improved subfilter-scale models from the HATS field data. *J. Atmos. Sci.*, **64**, 1694–1705.
- Hristov, T., C. Friehe, and S. Miller, 1998: Wave-coherent fields in air flow over ocean waves: Identification of cooperative behavior buried in turbulence. *Phys. Rev. Lett.*, **81**, 5245–5248.
- Hwang, P. A., 2004: Influence of wavelength on the parameterization of drag coefficient and surface roughness. *J. Oceanogr.*, **60**, 835–841.
- Janssen, P. A. E., 1999: On the effect of ocean waves on the kinetic energy balance and consequences for the inertial dissipation technique. *J. Phys. Oceanogr.*, **29**, 530–534.
- Lilly, D., 1967: The representation of small-scale turbulence in numerical simulation experiments. *Proc. IBM Scientific Computing Symp. on Environmental Sciences*, Yorktown Heights, NY, IBM, 195–210.
- Plant, W. J., 1982: A relationship between wind stress and wave slope. *J. Geophys. Res.*, **87**, 1961–1967.
- Rieder, K. F., and J. A. Smith, 1998: Removing wave effects from the wind stress vector. *J. Geophys. Res.*, **103** (C1), 1363–1374.
- Rotta, J., 1951: Statistische Theorie nichthomogener Turbulenz (Statistical theory of non-homogeneous turbulence). *Z. Phys.*, **129**, 547–572.
- Sjöblom, A., and A.-S. Smedman, 2003: Vertical structure in the marine atmospheric boundary layer and its implication for the inertial dissipation method. *Bound.-Layer Meteor.*, **109**, 1–25.
- Smedman, A.-S., U. Högström, H. Bergström, A. Rutgerström, K. Kahma, and H. Petterson, 1999: A case study of air–sea interaction during swell conditions. *J. Geophys. Res.*, **104**, 25 833–25 851.
- Smith, S. D., and Coauthors, 1992: Sea surface wind stress and drag coefficients: The HEXOS results. *Bound.-Layer Meteor.*, **60**, 109–142.
- Sullivan, P. P., and J. C. McWilliams, 2002: Turbulent flow over water waves in the presence of stratification. *Phys. Fluids*, **14**, 1182–1195.
- , T. W. Horst, D. H. Lenschow, C.-H. Moeng, and J. C. Weil, 2003: Structure of subfilter-scale fluxes in the atmospheric surface layer with application to large-eddy simulation modeling. *J. Fluid Mech.*, **482**, 101–139.
- , J. B. Edson, T. W. Horst, J. C. Wyngaard, and M. Kelly, 2006: Subfilter-scale fluxes in the marine surface layer: Results from the Ocean Horizontal Array Turbulence Study (OHATS). Preprints, *17th Symp. on Boundary Layers and Turbulence*, San Diego, CA, Amer. Meteor. Soc., 4.1. [Available online at http://ams.confex.com/ams/BLTAGFBioA/techprogram/paper_110884.htm.]
- , —, T. Hristov, and J. C. McWilliams, 2008: Large-eddy simulations and observations of atmospheric marine boundary layers above nonequilibrium surface waves. *J. Atmos. Sci.*, **65**, 1225–1245.
- Tong, C., J. Wyngaard, S. Khanna, and J. Brasseur, 1998: Resolvable and subgrid-scale measurement in the atmospheric surface layer: Technique and issues. *J. Atmos. Sci.*, **55**, 3114–3126.
- , —, and J. Brasseur, 1999: Experimental study of the subgrid-scale stresses in the atmospheric surface layer. *J. Atmos. Sci.*, **56**, 2277–2292.
- Vickers, D., and L. Mahrt, 1997: Fetch-limited drag coefficients. *Bound.-Layer Meteor.*, **85**, 53–79.
- Wyngaard, J. C., 2004: Toward numerical modeling in the “terra incognita.” *J. Atmos. Sci.*, **61**, 1816–1826.